Experimental Identification of the Mechanical Parameters of an Induction Motor Drive

Dejan D. Reljić, Dejan G. Jerkan
Department for Power, Electronic and Telecommunication Engineering
Faculty of Technical Sciences, University of Novi Sad
Novi Sad, Serbia
reljic@uns.ac.rs

Abstract **– In order to obtain fast dynamic response performance of an induction motor drive, the identification of mechanical parameters such as the drive inertia and the coefficients of friction, with a good accuracy, is highly desirable. They are essential for the design of the high-performance induction motor drive speed, as well as position controllers and speed observers, since a drive response is influenced not only by load disturbances but also by these mechanical parameters. Moreover, they are of great importance for the accurate dynamic modeling and simulation of various high-performance induction motor control strategies. In this paper an experimental off-line method for the mechanical parameters identification is presented. The method uses speed-time curve, obtained during the retardation test on the drive, with an appropriate mechanical losses model of the drive, and the mean squared error performance function based on a genetic algorithm (GA) approach, to obtain unknown mechanical parameters of the tested drive. The proposed method is verified by experiments.**

Keywords – genetic algorithm; induction motor; mechanical parameters identification; retardation test

I. INTRODUCTION

Induction motors, as a part of electrical drives, are by far the most widely used rotating electrical machines in many industrial applications [1]. The vast majorities of induction motors are usually used in a low-performance drives [2], such as pump and fan applications. However, induction motors are also used in a high-performance drives [2], such as machine tools, extruders, propulsion systems for the electrical vehicles, etc. In order to obtain fast dynamic response performance of an induction motor drive, the knowledge of electrical parameters is not enough [3]. The mechanical parameters are also of great importance.

The identification of the mechanical parameters, such as the drive inertia and the coefficients of friction, with good accuracy, is highly desirable. These parameters are crucial for the design of high-performance speed and position controllers. This is because a drive response is influenced not only by load disturbances but also by drive inertia and friction [4]. On the other hand, the identification of the mechanical parameters is also important for the accurate dynamic modeling and testing of various high-performance motor control strategies.

Many researchers have done a great number of researches on parameters identification of the induction motor. However, most of them are mainly focused on electrical parameters determination, while only a few of them are related to the mechanical parameters identification. In [4] an observer-based auto-tuning scheme with two adaptive controllers is used to separately adjust the drive inertia and friction torque to their correct value. In [5] a genetic algorithm (GA) is employed with the aim of determining the mechanical and electrical parameters of an induction motor. However, the most common and simple method of determining the moment of inertia is by performing a retardation test on the induction motor drive [6]-[11]. The retardation test is also suitable for the viscous friction coefficient identification [10], while the Coulomb friction is mainly neglected [9]. Nevertheless, the Coulomb friction may greatly affect the behavior of high precision drive systems [12]-[13]. In [7] an example of the dry torque determination using a progressive start-up experiment is presented. However, the proposed experiment in [7] is more related to static friction determination, but not the kinetic, i.e. Coulomb friction. The static friction is usually larger than the Coulomb friction [13].

The retardation test method is also used in this paper for the off-line mechanical parameters identification. The estimation of the drive inertia is similar to the procedure described in [6]-[11] with the exception that before the retardation test is done the flux density level in the motor is to be reduced. Thus, the speed-time curve is less influenced by electromagnetic transients. This results in more accurate drive inertia estimation. The Coulomb friction torque is estimated to be equal to the torque developed by the motor at the drive speed where the absolute value of the deceleration of the retardation curve begins to increase. Finally, a GA approach is employed to fit the proposed mechanical losses model of the drive (with previously estimated drive inertia and the Coulomb friction torque) to deceleration curve obtained by the retardation test. As a result, the drive inertia, the Coulomb friction torque and the unknown friction coefficients of the drive are obtained.

II. ESTIMATION OF THE DRIVE INERTIA

The moment of inertia is a measure of the body's resistance against a change of its rotational motion. It depends on the distribution of its mass relative to the axis of rotation [14]. The moment of inertia of a machine can be determined by an analytical calculation and by an experiment. Analytical computation is suitable during the design stage of the machine [11] but in the absence of the drive geometry details and used materials, it is ineffective for the whole drive inertia determination. Therefore, the drive inertia is usually determined by a direct experiment. The most common method of determining the drive inertia is by performing a test known as the retardation test on the drive [6]. The same method is used in this paper. However, in order to obtain a more accurate value of the drive inertia, the method is slightly modified in comparison to the ones described in [6]-[11].

The drive is run up to the speed above rated at no load. The supply voltage of the motor should be reduced as much as possible in order to reduce the flux density level in the motor to avoid electromagnetic transients (braking effect) after switching the power off, particularly for delta-connected windings. Then the motor's supply voltage is switched off. The drive slows down and comes to rest while speed-time curve is recorded. At any rotational speed ω, power P consumed in overcoming the mechanical losses is given by [6]-[11]:

$$P = \frac{d}{dt}\left(\frac{1}{2}\cdot J\cdot \omega^2\right) = J\cdot\omega\cdot\frac{d\omega}{dt}, \tag{1}$$

where J is the drive inertia. From the retardation test the slope of the deceleration curve $d\omega/dt$ is obtained at the speed ω_1 (usually ω_1 is the rated speed). Then the drive is reconnected to the power supply and run at the speed ω_1 by controlling the motor's supply voltage, and the electrical power input P_{01} to the motor is measured. As an approximation, the mechanical power P_1 at the speed ω_1 may be taken as:

$$P_1 = \left(P_{01} - P_{JS1} - P_{Fe1}\right)\cdot\left(1 - s_1\right), \tag{2}$$

where P_{JS1} is the stator Joule losses obtained from the measurement of the stator current and resistance, P_{Fe1} denotes the core losses, and s_1 is the slip at the speed ω_1 (the synchronous speed is known). The stray load losses in (2) are neglected, while the core losses, i.e. the stator core losses can be obtained by separation of no-load losses of the motor according to [15]. Now, using (1) and (2), the drive inertia can be calculated as:

$$J = \frac{P_1}{\omega_1\cdot\left|\left(\frac{d\omega}{dt}\right)_{\omega=\omega_1}\right|}. \tag{3}$$

Main problem in this method is that the mechanical losses cannot be estimated accurately because the rotor core losses in (2) are neglected. Besides, in the case of motors operated by PWM inverters, the core losses and the mechanical losses cannot be accurately separated because additional core losses appear due to higher order harmonics in the supply voltage. The core losses due to PWM harmonic voltages can be significant compared to a sinusoidal supply. These additional core loss components depend on the modulation index and on the inverter switching frequency [16]-[17]. The results in [16]-[17] show that core losses increase with decreasing modulation index, while increasing the switching frequency (above 5 kHz) has no significant effect on additional core losses, i.e. they remain almost constant independently of switching frequency. For those reasons it is rather difficult to achieve a good accuracy of the mechanical losses determination described by (2). However, the difficulties associated with additional core losses can be overcome if the motor in this test is supplied by the sinusoidal voltage instead by PWM inverter. This will significantly improve the accuracy of the drive inertia determination.

On the other hand, in order to provide higher level of accuracy, the drive inertia obtained from (3) will be tuned to more accurate value using the mechanical losses model of the drive and the GA approach. This will be discussed in the next sections.

III. THE MECHANICAL LOSSES MODEL

The mechanical losses in an induction motor drive are a result of mechanical losses in the induction motor and power losses in various parts of the transmission systems. Before the mechanical losses model of the tested drive system is established, the paper gives a short overview of each loss component.

A. Modeling the Induction Motor's Mechanical Losses

Mechanical losses in the induction motor occur due to friction in motor bearings and air movement in the motor. They are usually referred as bearings friction losses and windage and ventilation losses. The amount of these losses can be considerably large during a high-speed motor operation, and for totally enclosed fan-cooled motors.

The bearings are used in electrical machines to support the rotor and to keep the rotor centered in the stator [15], [18]-[19]. There are numerous different types of bearings that are used for electrical machines. The right selection depends on design requirements and operating conditions of the application [19]. In small machines ball bearings are commonly used, while in larger or heavily loaded machines roller bearings are typically used [19]. Regardless the type of bearings, they always contribute to the machine's overall friction power losses. The total friction in a bearing is the result of the rolling and sliding friction in the contact areas, between the rolling elements and raceways, between the rolling elements and a cage, and between the rolling elements and other guiding surfaces [20]. Friction is also generated by the lubricant drag and contact seals, if applicable [20]. The amount of friction depends on the loads, bearing type and size, operating speed, and properties and quantity of the lubricant [20]. The theoretical background of each of these sources of friction, including the mathematical formulation, is briefly explained in [20]-[21].

Friction is an extremely complex nonlinear phenomenon. Different models for the estimation of the bearings friction torque are available in literature. Five different models are described in [21] including the more advanced SKF bearing friction model [20]. Each of the models from [21] estimates the friction torque by grouping the individual sources together and quantifying them by empirical formulas. However, in this paper, the rotary Coulomb friction model [21] is adopted due to its simplicity. According to this model, the bearings friction torque T_b can be approximated as [20]-[21]:

$$T_b = 0.5 \cdot \mu \cdot F \cdot d \cdot \mathrm{sgn}(\omega), \tag{4}$$

where μ is the kinetic friction coefficient, F is the resultant bearing load, and d is the bearing bore diameter. Equation (4) is valid under certain conditions, such as: equivalent bearing load is 10% of the load rating, good lubrication, normal operating conditions (speed range 30-70% of the kinematically permissible speed) and no additional stress [21]. The kinetic friction coefficient μ is an experimentally determined constant. Its value depends on the bearing type and size, the bearing load, the load angle, and the rotational speed [21]. In [20] some typical values of the kinetic friction coefficient can be found.

It should be noted that at low-speed operation there is a considerable amount of mixed friction in bearings because rolling contacts are not yet separated by a lubricant film [20]. This is not included in (4). Low-speed drive operation is not considered in this paper.

A more complete evaluation of the bearings friction, including the influence of each contact areas and friction components, can be done using more advanced friction models and specialized software tools, but the manufacturer's specifications on the bearings and the lubricant are required. Usually, these data are difficult to be provided. For that reason, the model defined by (4) is more convenient because it only requires the knowledge of a few constants.

However, the bearings friction torque T_b can be estimated in a different way than it is proposed by (4). In [7] an example of the dry torque determination using a progressive start-up test experiment is presented. Nevertheless, the proposed experiment in [7] is more related to the static friction determination, but not the kinetic friction. This paper suggests that the bearings friction torque can be approximated as the torque developed by the unloaded induction motor at the speed ω_b at which the absolute value of the deceleration of the retardation curve begins to increase. Here it is assumed that from the speed ω_b the bearing friction torque starts to increase as speed decreases since a lubricant film is lost. Accordingly, the stator supply voltage at the rated frequency is reduced until the motor speed decreases to the value that is approximately equal to ω_b. Then, the bearings friction torque can be approximated as follows:

$$T_b = \frac{(P_b - P_{JSb}) \cdot (1 - s_b)}{\omega_b} = p \cdot \frac{P_b - P_{JSb}}{\omega_s}, \tag{5}$$

where P_b is the power absorbed by the motor when the motor speed is approximately equal to ω_b, P_{JSb} denotes the stator Joule losses obtained from the measurement of the stator current and resistance, s_b is the slip at speed ω_b, p is the number of pole pairs, and ω_s is the synchronous speed at the rated frequency. Note that the core losses in (5) are neglected since the stator voltage is small. To determine the speed ω_b speed-time curve, obtained during the retardation test, is needed.

Windage losses are friction losses associated with the friction between the rotor surface and the surrounding fluid, usually air within the air-gap [22]. This term is generally used to denote the loss due to fluid drag on a rotating body [23]. Windage losses are influenced by the rotor peripheral velocity, stator and rotor geometry and their surfaces roughness, the properties of the rotor's surrounding air and the length of the air-gap (the smaller the air-gap, the bigger the windage losses) [24]. Under the assumption that the rotor can be modeled as a rotating cylinder in an enclosure, the windage torque T_{w1} can be expressed as follows [22]:

$$T_{w1} = \frac{1}{32} \cdot k \cdot C_{M1} \cdot \pi \cdot \rho \cdot \omega^2 \cdot D_r^4 \cdot l_r, \tag{6}$$

where k is a roughness coefficient, C_{M1} is the torque coefficient, ρ is the density of air, D_r is the rotor diameter, and l_r is the rotor length. The torque coefficient C_{M1} depends on the Couette Reynolds number and it is determined by measurements [22].

The end surfaces of the rotor also create windage losses. Under the assumption that these parts can be modeled as discs rotating in free space, the windage torque T_{w2} can be expressed as follows [22]:

$$T_{w2} = \frac{1}{64} \cdot C_{M2} \cdot \rho \cdot \omega^2 \cdot (D_r^5 - D_{ri}^5), \tag{7}$$

where D_r is the outer diameter of the rotor, D_{ri} is the shaft diameter, and C_{M2} is the torque coefficient which, in contrast to (6), depends on the Reynolds number. However, the Couette Reynolds number and Reynolds number depend on the speed, which means that torque coefficients C_{M1} and C_{M2} are speed dependent.

The windage torque caused by the rotating parts of the machine is now the sum of (6) and (7):

$$T_w = T_{w1} + T_{w2}. \tag{8}$$

It follows from (6)-(8) that the windage torque increases with the square of the rotor speed, i.e. the windage power losses increases with the cubic of the rotor speed. This is of particular interest for high-speed motors.

Besides bearings friction losses and windage losses, ventilation losses also belong to mechanical losses. Induction motors are normally provided with a cooling system with the main objective to remove the heat generated by power losses in the motor. The cooling system consists of an internal shaft

mounted fan, or it can be driven by another motor (usually in variable-speed drives) [22]. The blades attached to the rotor short-circuiting ring have also a ventilating effect [25]. Windage losses and ventilation losses occur together. In [22] an experimental equation for the sum of windage and ventilation losses is given. These losses, expressed via the windage and ventilation torque T_{wv}, are:

$$T_{wv} = \frac{1}{4} \cdot k_{\rho} \cdot D_r^3 \cdot (l_r + 0.6 \cdot \tau_p) \cdot \omega \,, \tag{9}$$

where k_{ρ} is an experimental factor (typical values can be found in [22]), D_r is the rotor diameter, l_r is the rotor length and τ_p is the pole pitch. Equation (9) is valid for normal-speed motors, while for high-speed motors (7) and (8) have to be used.

B. Modeling the Drive's Mechanical Losses

The induction motor drive which is considered in this paper is shown in Fig. 1. The system consists of the three-phase cage induction motor (supplied by the power inverter) coupled to the wound-field synchronous machine. Besides, there is a flywheel system coupled directly to the induction motor shaft.

The drive from Fig. 1 is used to provide a variable frequency sinusoidal voltage source used for AC machines tests, as well as to test wound-field synchronous machine and flywheel energy storage system in renewable and distributed energy applications.

The total mechanical losses of the induction motor drive from Fig. 1 are a superposition of the mechanical losses from the both machines, and from flywheel and mechanical coupling. On the basis of the results obtained for the induction motor's mechanical losses formulation, the mechanical losses model for the synchronous machine will be established. These losses results from bearings and brush friction losses, and windage and ventilation losses.

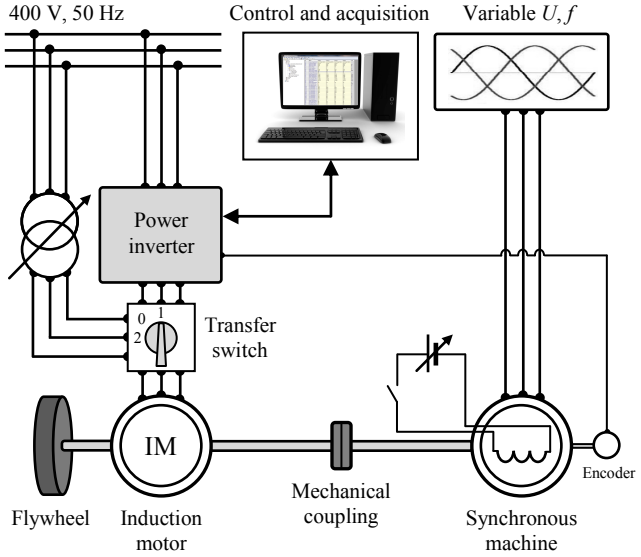

Figure 1. Induction motor drive system configuration.

Considering that a similar bearings type are used in both machines, and that they operate under similar working conditions, the bearings friction torque in the synchronous machine can be expressed as in (4). Brush friction usually has the Coulomb sliding friction characteristic. The torque to overcome the brush friction depends on the brush pressure, brush grade, contact area, and the condition of the slip rings [26]. Brush friction torque is a constant. It has been suggested in [26] to perform two retardation tests, one with brushes lifted and one without brushes lifted, to experimentally obtain brush friction torque. However, such a test has not been performed in this paper since the brush friction torque will be incorporated in the bearings friction torque of the tested drive. Besides, the sum of the bearings and brush friction torques can be approximately estimated as it is previously proposed for the bearings friction torque estimation for the induction motor.

The wound-field synchronous machine from Fig. 1 has a salient-pole rotor with a squirrel-cage winding distributed over the rotor. For that reason, this machine can be considered to have cylindrical-rotor with respect to windage and ventilation losses. Knowing the machine geometry, windage and ventilation torque can be calculated from (9).

The torque T_f of a thin flywheel disk caused by air resistance is described by [27]:

$$T_f = C_m \cdot \rho \cdot \omega^2 \cdot D_f^5 \,, \tag{10}$$

where C_m is the torque coefficient associated with the type of air flow (depends on the Reynolds number), ρ is the density of air, and D_f is the is the radius of the flywheel.

The air resistance torque of mechanical coupling losses can also be approximated by (10). However, it should be noted that the mechanical losses due to flywheel and mechanical coupling air resistance to motion are much lower than the windage and ventilation losses of the drive.

In order to obtain a more convenient mechanical losses model of the whole drive from Fig. 1, and to avoid the need for knowledge of the machines geometry, some modifications of the presented models will be carried out. The windage and ventilation losses model of the drive from Fig. 1 can be similarly expressed as (9), while for high-speed (6) and (7) have to be used. The flywheel and mechanical coupling air resistance to rotation can be modeled as (10). Taking (6), (7), (8), (9) and (10) into consideration, it is possible to replace these equations with their simpler and more convenient form. Namely, the paper proposes the corresponding torque T_{ρ} (sum of the mechanical losses due to windage and ventilation, and flywheel and mechanical coupling air resistance to rotation) to be modeled by the following expression:

$$T_{\rho} = b \cdot \omega^{(1+a \cdot \omega)} \,, \tag{11}$$

where a and b are coefficients of the drive. This model is consistent with the previous ones, except that the loss influence factors are expressed in a much more convenient way, through

the coefficients a and b. Substituting $a = 0$ in (11) the model (9) is obtained, while substituting $a \cdot \omega = 1$ (with different b values) in (11) the models (6), (7) and (10) are obtained. The term $a \cdot \omega$ in (11) is speed dependent and it is used as the replacement for coefficients associated with the type of air flow which depend on the Couette Reynolds and Reynolds numbers.

Using the estimated drive inertia J from (3), bearings and brush friction torque T_{bb} from (5), and the speed-time curve recorded during the retardation test, the unknown coefficients from (11) can be obtained on the basis of the Newton's second law of rotational motion for unloaded drive:

$$\frac{d\omega}{dt} = -\frac{T_{bb} + b \cdot \omega^{(1+a \cdot \omega)}}{J}. \tag{12}$$

The deceleration curve, obtained by performing the retardation test on the drive, is fitted to model (12) using the mean squared error performance function based on the GA approach. This will be discussed below.

IV. Genetic Approach to Mechanical Parameters Identification

In this section the model defined by (12) uses a GA approach to identify unknown coefficients a and b after a number of iterations that satisfy the fitness function and all constraints. Moreover, the GA is also used to tune the drive inertia J and the bearing and brush friction torque T_{bb} to more accurate values. This is done because the methods defined by (3) and (5) are influenced by the modeling and measurement errors. A brief introduction to the GA is presented.

A GA was introduced by J. H. Holland [28]. It is a model of machine learning which is based on the natural processes of selection and evolution. The GA uses a stochastic approach which operates on individuals of a population, applying the principle of survival of the fittest which then evolves toward the solution of the selected problem [28]. The basic principles of the GA are quite simple. The first step is the selection of individuals from an initial population. The individuals carry chromosomes which are potential solutions to the selected problem. The algorithm usually selects individuals that have better fitness values. The second step is genetic manipulation of the selected individuals by crossover and mutation methods, including elitist selection. This results in new population which is better than the previous generation. At each next step, the GA uses the current population to create the next generation. The algorithm stops when the stopping criteria are met.

In this paper the main goal of the GA is to find the mechanical parameters of the drive from the model defined by (12). The fitness function is defined in such a way that the fitness values are minimized:

$$fit = mse\left(\frac{\frac{d\omega_m}{dt}(i) - \frac{d\omega}{dt}(i)}{\frac{d\omega_m}{dt}(i)}\right), \tag{13}$$

where *fit* denotes the fitness function, *mse* stands for the mean squared error, $d\omega_m/dt(i)$ are the elements of the vector which is composed of the angular deceleration points obtained by the retardation test on the drive, and $d\omega/dt(i)$ are the vector's elements of the angular deceleration points estimated by (12).

Equation (13) is an optimization problem which has been solved in this paper by the GA solver using Matlab's Optimization Toolbox [29]. The GA is a relatively new optimization technique, but it has been proved as an effective method for the process optimization. Yet, options for the GA solver need to be carefully selected. Otherwise, the GA method would get stuck in local minima. The knowledge about the proper selection of the GA parameters has a rather empirical background and some recommendations can be found in [30]. Table I provides a quick overview of the most important selected parameters and methods provided by Matlab's Optimization Toolbox that has been used in this paper for mechanical parameters identification.

The size of the population depends on the problem complexity. The problem of optimal population size has been studied in literature, but a general rule cannot be applied to every problem. In this paper population size has been tuning until reaching reasonable value of the fitness function (13).

Furthermore, it is particularly important to specify an initial population of the GA. If not, Matlab creates a random initial population using a creation function which can lead to bad performance of the algorithm. The initial values of the drive inertia J and the bearings and brush friction torque T_{bb} can be calculated according to (3) and (5), respectively, while the initial value of the coefficient a can be selected to be zero. The initial value of the coefficient b can be roughly selected according to the mechanical losses data of the motor (drive) obtained by no-load test [15]. This ensures diversity in the GA and provides the GA to converge quickly for finding near-optimal solution to the problem.

The fitness scaling option is Rank, which scales the raw scores based on the rank of each individual.

Selection function selects individuals, i.e. the parents from the population, based on their scaled values from the fitness scaling function. In this GA, the Stochastic uniform function has been selected to perform the selection.

TABLE I. Parameterization of the GA

Options	Values, methods
Population size	50
Fitness scaling	Rank
Selection function	Stochastic uniform
Reproduction	Elite count: 2; Crossover fraction: 0.8
Mutation function	Adaptive feasible
Crossover function	Heuristic, ratio: 2
Stopping criteria	Generations: 100; Stall generations: 50

Reproduction determines method which is used for each new generation creation. Elite count specifies the number of individuals that will be moved to the next generation. Crossover fraction defines the fraction of the next generation produced by a crossover manipulation. The remaining individuals in the next generation will be produced by mutation. Elite count has been selected to be 2 and Crossover fraction 0.8. This provides good results.

Mutation function provides genetic diversity by preventing the population of chromosomes from becoming similar to each other. The Adaptive feasible function has been specified to perform the mutation.

Crossover function combines two individuals in order to generate a new individual for the next generation. Several crossover functions have been tested. Heuristic function with ratio 2 gives satisfactory results.

The GA is iterated until a termination condition has been reached. Terminating conditions are the maximum number of iterations (100) and stall generations (50).

V. Experimental Results

The mechanical parameters were determined on the drive from Fig. 1. The cage induction motor has following rated data: 20 kW, 380 V, 40 A, 50 Hz, 1455 rpm, delta-connected windings. For this experiment the motor was connected to the sinusoidal three-phase supply 400 V, 50 Hz (transfer switch in Fig. 1 was in position 2) though the variac which controls the supply voltage. An optical encoder was attached to the shaft for speed measurement. During tests, the drive was unloaded, i.e. the synchronous machine (Fig. 1) was not excited.

Before the retardation test was done, the no-load test (at the motor's rated frequency) [15] of the drive was performed to separate the mechanical losses from the core losses. The result of this experiment is shown in Fig. 2.

For the retardation test the motor was supplied with the reduced voltage at the rated frequency and was run under the steady-state on the unloaded drive. The motor (drive) speed had to be slightly over rated speed and was set to 1490 rpm (156 rad/s), while the supply voltage was 113 V. It was necessary to wait some time to stabilize the temperature of the drive's bearings and then the motor was disconnected from the power supply and the speed-time curve was recorded. The result of the retardation test is shown in Fig. 3. From Fig. 3 a time derivative of the rotating speed can be obtained (Fig. 4). The specific part of the angular deceleration curve at low speeds is enlarged in Fig. 4. After the retardation test was done, the motor was reconnected to the power supply and ran at the near of its rated speed by controlling the motor's supply voltage. The motor (drive) speed was set to 1450 rpm (ω_1=151.8 rad/s), while the supply voltage was 57 V. The electrical input power to the motor P_{01}, the stator current I_{01} and the stator winding resistance R_s were measured. The core losses P_{Fe1} were read on the curve of Fig. 2, while the angular deceleration $d\omega/dt$ at the speed ω_1 was read on the curve of Fig. 4. The drive inertia was calculated according to (3). Table II describes the results obtained on the drive. The value of the drive inertia will be used in initial population of the GA.

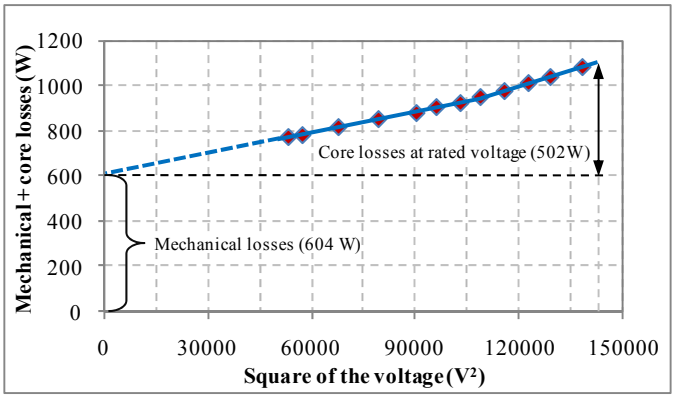

Figure 2. Separation of the no-load losses.

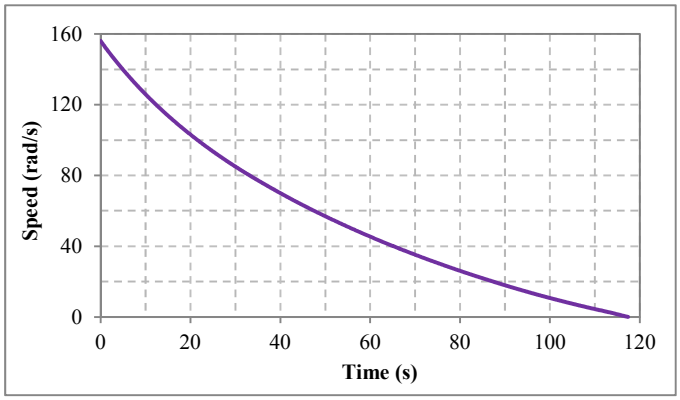

Figure 3. Retardation test on the drive.

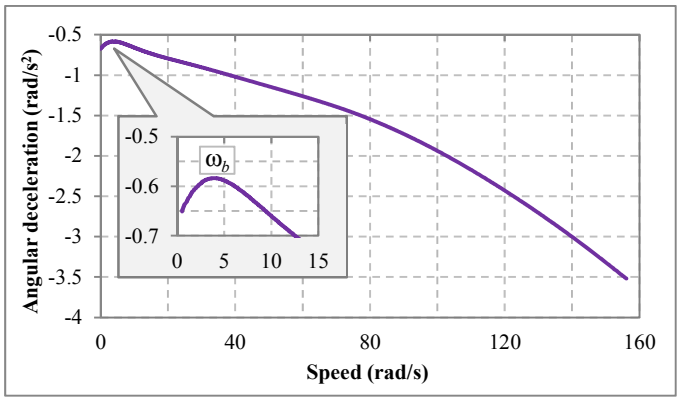

Figure 4. Angular deceleration curve.

TABLE II. The Results Obtained from the Retardation Test

ω_1 (rad/s)	$(d\omega/dt)_{\omega=\omega_1}$ (rad/s²)	P_{01} (W)	I_{01} (A)	R_s (mΩ)	P_{Fe1} (W)	P_1 (W)	J (kgm²)
151.8	− 3.379	602	7.37	311	10	556	1.084

The bearings and brush friction torque T_{bb} can be easily approximated as described in (5) for the bearings friction torque T_b determination. However, it is previously necessary to identify the speed ω_b at which the absolute value of the angular deceleration of the retardation curve begins to increase. This

characteristic speed was readily found on angular deceleration curve and its value is $\omega_b = 3.87$ rad/s (enlarged part of the curve in Fig. 4). Thereafter, the stator supply voltage was being reduced until the motor speed was decreased to the value of ω_b. Nevertheless, the proposed procedure was associated with the static stability problem of the drive system and exact value of ω_b could not be achieved. For that reason electrical input power to the motor P_b, the stator voltage U_b, current I_b and the stator winding resistance R_s were measured for a few operating points slightly above the speed ω_b, and then the bearings and brush friction torque T_{bb} was estimated for the speed ω_b by an extrapolation procedure. This procedure involved the use of (5) for each achieved operating point in order to obtain the torque T developed by the motor. Afterwards, the bearings and brush friction torque T_{bb} was extrapolated. It should be noted that (5) is valid for low-speed drive operation, as was the case here. The results are summarized in Table III.

Eventually, the mechanical parameters identification was undertaken using the proposed GA and the fitness function (13), including angular deceleration curve from Fig. 4, whereby the estimated drive inertia J and the bearings and brush friction torque T_{bb} from Table II and Table III, were used as initial values. Since the rotor core losses in (2) and (5) were neglected, as well as the windage and ventilation losses in the bearings and brush friction torque estimation, it was expected that the actual values of the drive inertia and the bearings and brush friction torque were lower than the previously estimated ones. With regard to this, previously estimated values of the drive inertia J and the bearings and brush friction torque T_{bb} were specified as upper bounds on these variables. The initial value of the coefficient a from (11) was selected to be zero, while the initial value of the coefficient b was roughly selected according to the mechanical losses data of the motor (drive) obtained by no-load test (Fig. 2), e.g. 0.024 (Table IV). The initial value of the coefficient a was specified as lower bound on this variable, while the coefficient b was specified as upper bound on this variable. The GA was run several times until the mechanical parameters set was obtained (Table IV). The objective function value of the best solution is $1.9809 \cdot 10^{-4}$.

TABLE III. THE RESULTS OF THE BEARING AND BRUSH FRICTION TORQUE ESTIMATION

ω (rad/s)	P_b (W)	U_b (V)	I_b (A)	R_s (mΩ)	T (Nm)	T_{bb} (Nm)
9.74	184.2	25.17	11.67	311	0.903	
7.64	169.4	24.17	11.20	311	0.830	-
5.12	153.3	23.00	10.70	311	0.749	
3.87	-					0.709

TABLE IV. THE RESULTS OBTAINED BY THE GA APPROACH

Mechanical parameters	J (kgm^2)	T_{bb} (Nm)	a	b
Initial values	1.084	0.709	0	0.024
Final values	1.078	0.6544	0.00098	0.0093

The mechanical losses components of the tested drive, obtained by the proposed methods, are shown in Fig. 5. It should be noted that low-speed drive operation was not considered in this paper, i.e. it is not covered by the proposed mechanical losses model. It is assumed that below the speed ω_b the bearings friction torque starts to increase as speed decreases since a lubricant film is lost. This is not included in the proposed bearings and brush friction torque model. For that reason the mechanical parameters set from Table IV are not valid below speed ω_b (Fig. 4). However, it is interesting to calculate the mechanical losses of the drive (P_m) from Fig. 1 at no-load (ω=157 rad/s) according to the proposed model and the loss coefficients obtained by the GA approach (Table IV):

$$P_m = \left(T_{bb} + b \cdot \omega^{(1+a\cdot\omega)}\right) \cdot \omega = 602 \text{ W} . \qquad (14)$$

The result of (14) is in good agreement with the experimental result obtained by no-load test of the drive (Fig. 2).

In order to validate the proposed mechanical losses model and methods for the estimation of the mechanical parameters of the drive, additional experiments were carried out. The motor was connected to a 60 Hz source at reduced voltage (transfer switch in Fig. 1 was in position 1 and the motor was connected to power inverter) and was run under steady-state on the unloaded drive. Then the retardation test was performed. The result of this experiment is shown in Fig. 6, where it is also shown the estimated retardation curve obtained according to (12) with the parameters from Table IV.

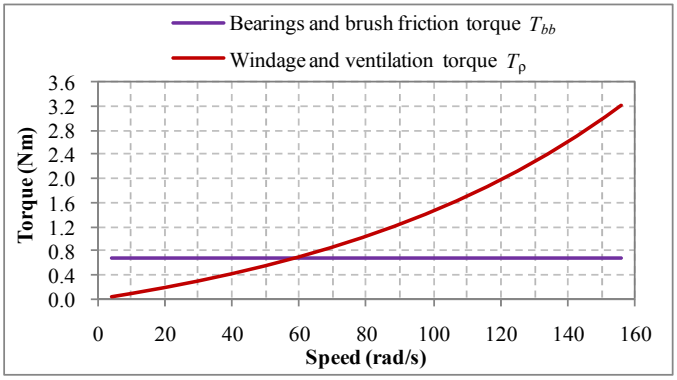

Figure 5. The mechanical losses components of the tested drive.

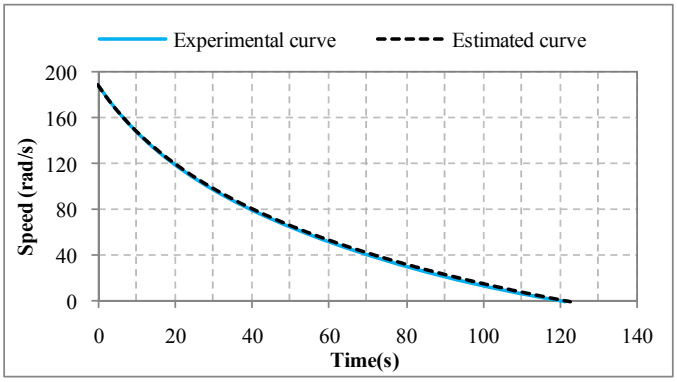

Figure 6. Retardation test on the drive at 60 Hz.

As shown in Fig. 6 the estimated retardation curve is in a good agreement with the experimental curve.

Another experiment was performed on the drive from Fig. 1 with the flywheel removed. The flywheel is a solid, uniform disk which has inertia of 0.1454 kgm^2. Since the flywheel was directly coupled to the motor shaft, after it was removed, the drive inertia referred to the motor shaft is 0.9336 kgm^2. In this experiment the motor was supplied with the reduced voltage at the rated frequency and was run under the steady-state on the unloaded drive. At that moment the retardation test was performed. The result of this experiment is shown in Fig. 7. The same figure shows the estimated retardation curve obtained according to (12) with the parameters from Table IV, but with the drive inertia of 0.9336 kgm^2. As can be seen in Fig. 7, there is a certain discrepancy between the experimental and the estimated retardation curves. This disagreement is noticeable at lower speeds regions. The reason for discrepancy between results can be found in the resultant bearings load. Namely, when the flywheel was removed, according to (4) the resultant bearings load was decreased. Besides, disagreement also exists because there were no the mechanical losses due to flywheel air resistance to motion. To correct the estimated retardation curve, the bearings and brush friction torque was estimated again employing the proposed GA method, while the other mechanical parameters (a and b from Table IV) were not changed. The results are shown in Fig. 8. The estimated retardation curve, obtained according to (12) with new estimated value of the bearings and brush friction torque (0.62 Nm), shows good agreement with the experimental curve, validating the effectiveness of the proposed method.

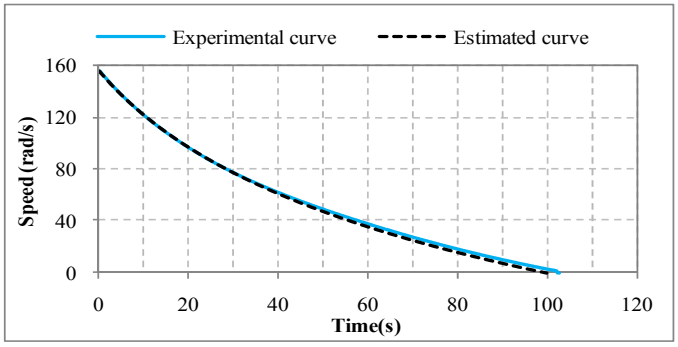

Figure 7. Retardation test on the drive at 50 Hz without flywheel.

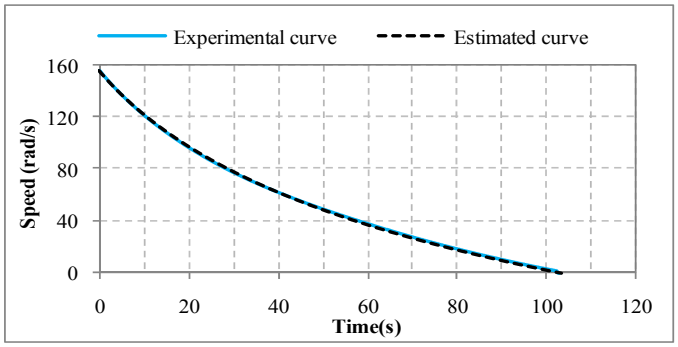

Figure 8. Retardation test on the drive at 50 Hz without flywheel - Corrected estimated curve.

VI. Conclusion

In this paper, the experimental method for the identification of the mechanical parameters of the induction motor drive was presented. The method is based on the improved retardation test with the help of the GA.

In addition, the mechanical losses model of the tested drive was established. Novel modeling approach of the windage and ventilation losses was introduced. The model is much more suitable for practical use, compared to the ones that can be found in literature, since it does not require a detailed knowledge of the machines geometry.

The effectiveness of the proposed methods was demonstrated by experiments. Good agreements were found between the estimated and the experimental results.

Future researches should follow up on improving the mechanical losses model of the drive system in low-speed regions and at standstill.

Acknowledgment

This work was supported by the Ministry of Education, Science and Technological Development of the Republic of Serbia under project III42004.

References

[1] S K Bhattacharya, Electrical machines, 3rd ed., New Delhi, India: Tata McGraw-Hill Education, 2009.

[2] B. Blanusa and B. Knezevic, "Simple Hybrid Model for Efficiency Optimization of Induction Motor Drives with Its Experimental Validation," Advances in Power Electronics, vol. 2013, Article ID 371842, pp. 1-8, February 2013.

[3] H. Sediki, A. Bechouche, D. O. Abdeslam, S. Haddad, "ADALINE approach for induction motor mechanical parameters identification," Mathematics and Computers in Simulation, vol 90, pp. 86-97, April 2013.

[4] S. M. Yang, Y. J. Deng, "Observer-Based Inertial Identification for Auto-Tuning Servo Motor Drives," IEEE Industry Applications Conference, vol. 2, pp. 968-972, Oct. 2005.

[5] F. Alonge, F. D'Ippolito, G. Ferrante, F.M. Raimondi, "Parameter identification of induction motor model using genetic algorithms," Control Theory and Applications, IEE Proceedings, vol. 145(6), pp. 587–593, Nov. 1998.

[6] S.K. Pillai, A first course on electrical drives, 2nd ed., New York: Wiley, 1989.

[7] Fouad Giri, AC Electric Motors Control : Advanced Design Techniques and Applications, New York: Wiley, 2013.

[8] M.V. Deshpande, Electric Motors: Applications and Control, New Delhi, India: Phi Learning, 2010.

[9] G. K. Dubey, Fundamentals of Electrical Drives, 2nd ed., India: Alpha Science International, 2001.

[10] W. Saekok, P. Lumyong, "Characteristics Evaluation of 3 Phase Induction Motors Based on an Acceleration Method with Increasing Moment of Inertia Technique," SDEMPED 2003, pp. 93-98, August 2003.

[11] I. D. Ilina, "Experimental determination of moment to inertia and mechanical losses vs. speed, in electrical machines," 7th International Symposium on Advanced Topics in Electrical Engineering, pp. 1-4, May 2011.

[12] L. Borello, M. D. L. Dalla Vedova, "Dry Friction Discontinuous Computational Algorithms," International Journal of Engineering and Innovative Technology (IJEIT), vol. 3(8), pp. 1-8, February 2014.

[13] I. Virgala, P. Frankovský, M. Kenderová, "Friction Effect Analysis of a DC Motor," American Journal of Mechanical Engineering, vol 1(1), pp. 1-5, 2013.

[14] (2014) LD DIDACTIC Group webpage. [Online]. Available: http://www.ld-didactic.de/literatur/hb/e/p1/p1452_e.pdf

[15] IEEE Standard Test Procedure for Polyphase Induction Motors and Generators, IEEE Std 112-2004

[16] T. L. Mthombeni, P. Pillay, "Lamination Core Losses in Motors With Nonsinusoidal Excitation With Particular Reference to PWM and SRM Excitation Waveforms," IEEE Transactions on Energy Conversion, vol. 20, No. 4, pp. 836-843, December 2005.

[17] S. Khomfoi, V. Kinnares, P. Viriya, "Influence of PWM characteristics on the core losses due to harmonic voltages in PWM fed induction motors," Power Engineering Society Winter Meeting, vol. 1, pp. 365-369, Jan. 2000.

[18] G. P. Shultz, Transformers and Motors, 1st ed., USA: Elsevier Science, 1997.

[19] (2013) SKF Rolling bearings and seals in electric motors and generators.

[20] (2012) SKF rolling bearings catalogue.

[21] J. Croes and S. Iqbal, D2.1 Document 3: Literature Survey: bearing losses, Energy Software Tools for Sustainable Machine Design EC - 7th Framework Programme, K.U.Leuven, 2009.

[22] J. Pyrhonen, T. Jokinen and V Hrabovcova, Design of Rotating Electrical Machines, 1st ed., Chippenham, Great Britain: John Wiley & Sons, 2008.

[23] W. Tong, "Numerical Analysis of Flow Field in Generator End-Winding Region," International Journal of Rotating Machinery, vol. 2008, Article ID 692748, pp. 1-10, 2008.

[24] Improving the Efficiency of Squirrel Cage Induction Motors: Technical and Economical Consideration, The Swedish Energy Agency publication. [Online]. Available: http://www.energimyndigheten.se/PageFiles/18106/Elmotorer%20Beakt ande%20803970.pdf

[25] N. Voicu, L. Dumitriu, M. Iordache, D. Niculae, "Modeling of the Induction Motor Ventilation by Electric Circuits," The Scientific Bulletin, Series C, vol. 71 (4), pp. 175-182, 2009.

[26] H. A. Toliyat, G. B. Kliman, Handbook of Electric Motors, USA: CRC Press, 2004.

[27] K. Ludlu, "Optimizing Flywheel Design for use as a Kinetic Energy Recovery System for a Bicycle," Senior Theses, Pomona College, Claremont, California, 2013.

[28] J. H. Holland, Adaptation in Natural and Artificial Systems, 2nd ed., Cambridge, MA: MIT Press, 1992.

[29] MATLAB and Optimization Toolbox, The MathWorks, Inc., Natick, Massachusetts, United States.

[30] Z. Michalewicz, Genetic Algorithms + Data Structures = Evolution Programs, 3rd ed., Berlin, Germany: Springer-Verlag, 1996.